The heat energy dissipated in a control volume to correlate the crack propagation rate in stainless steel specimens

G. Meneghetti, M. Ricotta
University of Padova, Italy
giovanni.meneghetti@unipd.it, http://orcid.org/0000-0002-4212-2618
mauro.ricotta@unipd.it, http://orcid.org/0000-0002-3517-9464

ABSTRACT. Metallic materials dissipate thermal energy when subjected to fatigue. Some of them, due a favorable combination of thermo-physical material properties, exhibit a significant temperature rise, which can be easily measured in-situ by means of thermocouples or infrared cameras. The heat energy dissipated in a unit volume of material per cycle (the Q parameter) has proven to be effective as a fatigue damage index in case of AISI 304L plain and notched specimens. Originally conceived and applied as a point-related quantity, recently Q has been averaged at the tip of propagating fatigue cracks (the Q* parameter) in order to correlate crack growth data gathered from fracture mechanics tests. The use of Q* seems interesting because (i) it can be evaluated in-situ from infrared temperature maps and (ii) crack acceleration due to excessive plasticity is likely to be accounted for.

KEYWORDS. Fracture Mechanics; Crack tip plasticity; Energy methods; Fatigue; Temperature.

Citation: Meneghetti, G., Ricotta, M., The heat energy dissipated in a control volume to correlate the crack propagation rate in stainless steel specimens, Frattura ed Integrità Strutturale, 41 (2017) 299-306.

Received: 28.02.2017
Accepted: 03.05.2017
Published: 01.07.2017

INTRODUCTION

In the last years the authors proposed [1] to use the heat energy to rationalise the fatigue behaviour of plain and bluntly notched specimens made of AISI 304L stainless steel subjected to push-pull, constant amplitude [2,3] and two load level [4] fatigue tests. The mean stress influence in fatigue has also been taken into account [5]. The proposed approach assumes the heat energy dissipated in a unit volume of material per cycle, Q, as a fatigue damage index, that can be readily evaluated by means of temperature measurements performed at the crack initiation point. Originally conceived and applied as a point-related quantity, Q can hardly correlate fatigue test results generated from cracked specimens. Rather, it should be averaged inside a material dependent structural volume V_c [6]. The approach is sketched in Fig. 1a. In a previous paper it was demonstrated that the specific energy per cycle dissipated as heat is approximately equal to the plastic strain hysteresis energy, which drives fatigue crack propagation according to ref. [7].

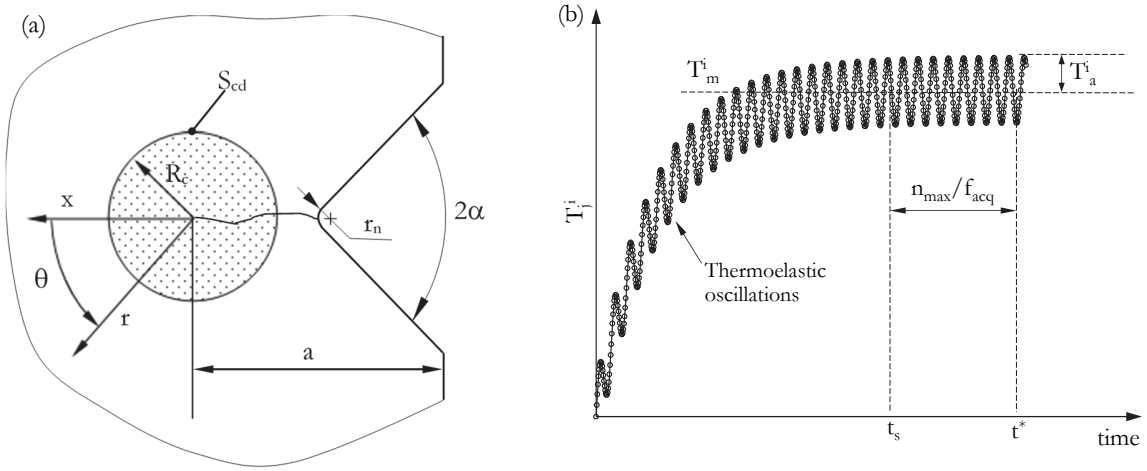

Figure 1: A propagating fatigue crack and the assumed shape of the structural volume V_c where the heat energy is to be averaged (a) and time-variant temperature for i-th pixel (b).

The averaged heat energy generated inside the structural volume can be evaluated as follows:

$$Q^* = \frac{1}{V_c}\int_{V_c} Q \cdot dV_c \Rightarrow = \frac{1}{f_L V_c}\cdot \int_{S_{cd}} h \cdot dS_{cd} \tag{1}$$

where h is the heat flux existing at a point along the boundary of V_c, S_{cd}, through which heat energy is extracted by conduction. It is worth noting that Eq. (1) is valid under the hypothesis that the heat is extracted from V_c only by conduction, which is not true, strictly speaking. However, it has been demonstrated that conduction is by far the most active heat dissipation mechanism in standard laboratory testing conditions [8]. The heat flux can be evaluated from the thermal gradients calculated from infrared temperature maps; therefore, referring to a two-dimensional problem, Eq. (1) can be written as follows [8]:

$$Q^* = -\frac{1}{f_L V_c}\cdot \lambda \cdot \chi \cdot R_c \cdot \int_{-\pi}^{+\pi} \left.\frac{\partial T_m(r,\theta)}{\partial r}\right|_{r=R_c} \cdot d\theta \tag{2}$$

$T_m(r,\theta)$ being the mean temperature, measured when the thermal equilibrium with surroundings is reached. Fig. 1b reports a typical temperature vs time acquisition at a point of a specimen or component after a fatigue test has started. If the temperature field is monitored by means of an infrared camera, Fig. 1b is the pixel-by-pixel temperature vs time history and it shows that temperature increases until the mean temperature level stabilizes, while the alternating component due to the thermoelastic effect still exists. If we consider a sampling window taken after thermal equilibrium with the surroundings is achieved (between t_s and t* in Fig. 1b), the mean temperature T^i_m for i-th pixel is defined as follows:

$$T_m^i = \frac{\sum_{j=1}^{n_{max}} T_j^i}{n_{max}} \tag{3}$$

where T_j^i are the temperature data acquired at a sampling rate f_{acq} and $n_{max} = f_{acq}\cdot(t^* - t_s)$ is the number of picked-up samples between the time t_s (j=1) and the time t* (j=n_{max}).

Eq. (2) is based on the radial temperature gradient, therefore it has been referred as spatial gradient technique. An alternative method to evaluate Q* has also been proposed, which is based on the cooling gradient measured after the machine test has been stopped and therefore it has been referred as cooling gradient technique [8]. However, the latter method has not been applied here.

The aim of the present paper is to use the parameter Q* to correlate crack growth data generated from tension-compression axial fatigue tests on specimens machined from 4-mm-thick, hot-rolled AISI 304L steel plates. The plan of

the paper is as follows: to estimate the structural volume size R_c, to present the crack growth experiments and temperature measurements and finally to use Q* as crack driving force.

MATERIAL AND TESTING METHODS

Specimens were prepared from 4-mm-thick, hot-rolled AISI 304L stainless steel specimens. The mechanical properties and the chemical composition are reported in Tab. 1.

$R_{p0.2\%}$ (MPa)	R_m (MPa)	A (%)	σ_{A-1} (MPa)	HB	C (%)	Mn (%)	Si (%)	Cr (%)	Ni (%)	P (%)	S (%)	N (%)
279	620	57	202	170	0.026	1.470	0.370	18.100	8.200	0.034	0.001	0.058

Table 1: Mechanical properties and chemical composition of the AISI 304L stainless steel.

The specimens' geometry is reported in Fig. 2a-b, which shows the crack starter, consisting of a sharp, 8-mm-deep V-notch. Both specimens' surfaces were polished by means of emery papers starting from grade 80 up to grade 4000; afterwards, a black paint was applied to one specimen's surface in order to increase the emissivity in view of the infrared thermal measurements. Push-pull (R=-1), constant amplitude, load controlled crack propagation tests were conducted on a servo-hydraulic Schenck Hydropuls PSA100 fatigue test machine equipped with a TrioSistemi RT3 digital controller (load capacity 100 kN). Load frequencies ranging between 4 and 40 Hz were adopted, depending on the applied stress level. After a fatigue test started, a crack initiated at the notch tip and it was propagated to a total initial crack length of approximately a=9 mm (according to Fig. 1a). Afterwards, crack growth experiments started. The temperature field was measured by means of a FLIRSC7600 infrared camera, having a 50-mm focal lens and equipped with an analog input interface, which was used to synchronize the force signal coming from the load cell with the temperature signal measured by the infrared camera. The infrared camera had a spectral response range from 1.5 to 5.1 μm, a noise equivalent temperature difference (NETD) < 25 mK, and operated at a frame rate f_{acq} equal to 200 Hz. A 30-mm spacer ring was adopted to improve the spatial resolution up to 20 or 23 μm/pixel. As a result, the Field of View (FoV) was reduced to 320x256 pixels, which corresponds to a minimum of 6.4 mm x 5.1 mm and a maximum of 7.4 mm x 5.9 mm.

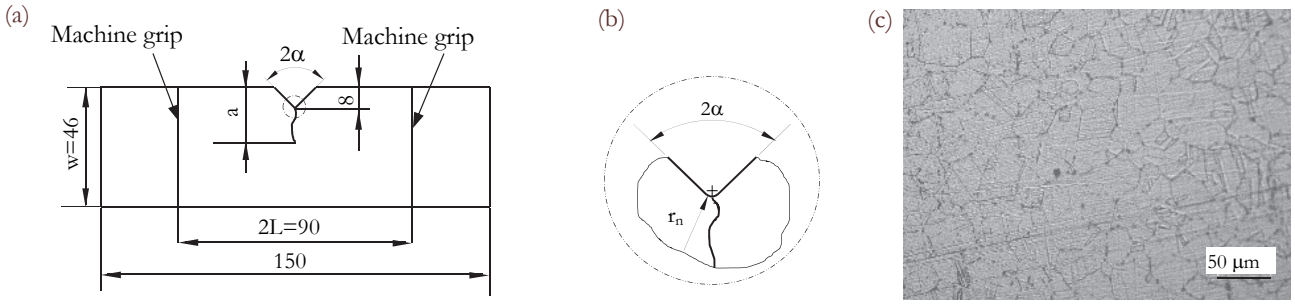

Figure 2: specimen's geometry (r_n=0.1 mm for 2α=45°, r_n=0.15 mm for 2α=90°; thickness is 4 mm; dimensions in mm) (a,b) and AISI 304L austenitic microstructure (c).

In order to evaluate Q* at a given crack length during the fracture mechanics experiments, a trigger signal was manually sent to the infrared camera to start the acquisition of the thermal images at a frame rate f_{acq}=200Hz for a duration of 5s, translating into 1000 acquired images. Such temperature maps were first processed by using the FLIR MotionByInterpolation tool to allow for the relative motion compensation between the fixed camera lens and the moving specimen subject to cyclic loads (the displacements to compensate ranged from 6 to 20 pixels within the FoV, depending on the stiffness of the specimen). To perform successfully the motion compensation, the force signal coming from the load cell must be sampled synchronously with the thermal images. After that, the spatial distribution of the mean temperature $T_m(r,\theta)$ was calculated by averaging the available 1000 temperature maps according to Eq. (3) and by means of the ALTAIR 5.90.002 commercial software; finally, the Q* parameter was evaluated by applying Eq.(2).
The crack length was measured by means of a AM4115ZT Dino-lite digital microscope operating with a magnification ranging from 20x to 220x. The microscope and the infrared camera monitored the opposite surfaces of the specimens; in

particular, the microscope images were used to single-out the crack tip position, which was subsequently reported in the infrared thermal images. A total number of 10 specimens was fatigue tested.

THE STRUCTURAL VOLUME SIZE V_c

The experimental procedure to evaluate the structural volume size R_c (see Fig. 1a) was a tricky point, which was tackled in [9] and is summarized here. The underlying concept to evaluate the structural volume size R_c, thought of as a material property for a given applied nominal load ratio, is widely adopted in notch fatigue [6,10-14] and, if formalized in the present case, it states that the averaged energy Q* must be the same at the conventional fatigue limit, whatever the geometrical features involved. Alternatively stated, the characteristic energy Q* at the fatigue limit of a plain and a notched (either blunt or severe) specimen must be the same.

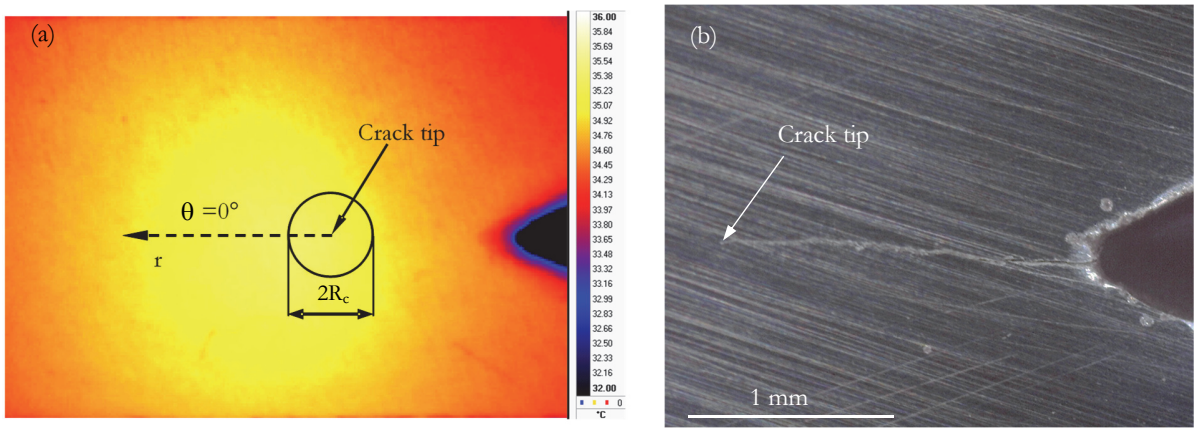

Figure 3: temperature field for a specimens having a 9.803-mm-long crack (see crack length definition 'a' in Fig. 1a), loaded at $\Delta K=32.7$ MPa·m$^{0.5}$, $f_L=35$ Hz (a), and microscope image of the fatigue crack taken on the opposite surface (b).

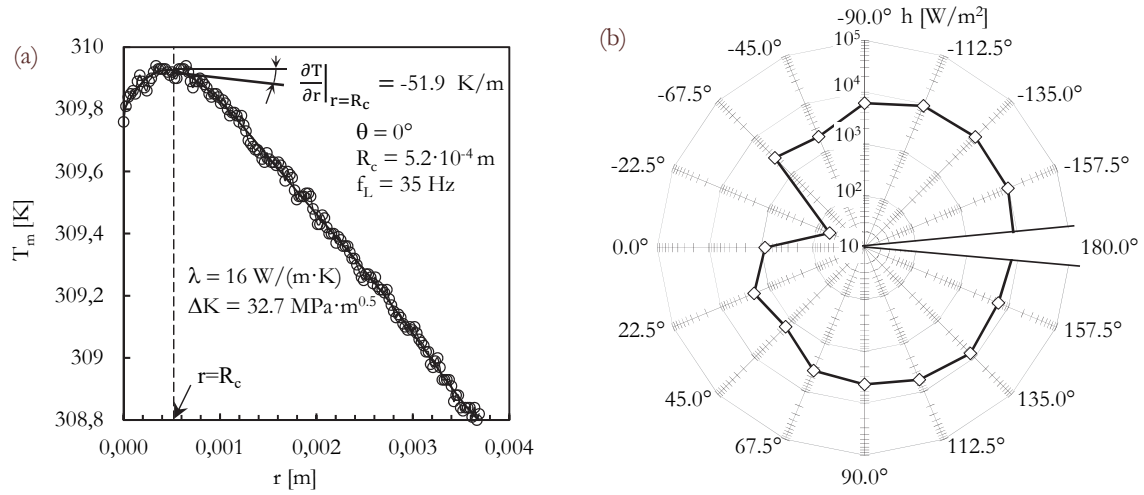

Figure 4: Radial temperature profile (a) and specific heat flux distribution measured along the boundary of V_c (b), during tension-compression fatigue test with a=9.803 mm, $\Delta K=32.7$ MPa·m$^{0.5}$, $f_L=35$ Hz.

Unfortunately, at the fatigue limit of the present cracked specimens, the thermal rise close to the crack tip was vanishingly small in relation to the thermal accuracy of the available infrared camera. Therefore, calibration of R_c was performed at a fixed finite-life, rather than at the fatigue limit. The chosen reference fatigue life was on the order of 10^5 cycles and the calibration procedure is explained in the following with reference to a single fatigue test. A specimen was pre-cracked to obtain a total crack length a=9.803 mm (according to Fig. 1a). Fig. 3a shows the temperature field calculated by averaging the 1000 available frames, after the motion compensation algorithm has been applied. The crack tip position (see Fig. 3b) could be determined from the digital microscope image captured on the opposite surface. The number of cycles to

separate the specimen starting from the configuration shown in Fig. 3 was ΔN_f=69840 cycles. The relevant temperature profile evaluated at θ=0° and the heat flux h calculated along the boundary of V_c are reported in Fig. 4a and Fig. 4b, respectively.

For the same fatigue life, the characteristic energy of plain specimens made of the same material and loaded with the same load ratio can be found in ref. [15], to which the reader is referred, and is equal to Q=Q*=0.66 MJ/(m³•cycle). As a final step, the control radius R_c was iteratively varied in Fig. 3a until the averaged heat loss Q* calculated inside V_c by means of spatial gradient technique – Eq. (2) - was equal to the characteristic value 0.66 MJ/(m³•cycle). The result was R_c=0.65 mm. By repeating such a procedure using additional three specimens, the results reported in Tab. 2 were obtained, where a mean value R_c=0.52 mm was calculated.

a[1] (mm)	ΔN_f (/)	Q*[2] (MJ/(m³ cycle))	ΔK (MPa$\sqrt{m}$)	R_c[1] (mm)
9.803	69840	0.66	32.7	0.65
19.035	82001	0.61	33.0	0.45
14.969	62221	0.69	35.0	0.42
8.475	46263	0.80	38.0	0.55
			Mean value	0.52

[1] see Fig. 1a; [2] From Eq. (2)

Table 2: Experimental value of the structural volume size of the AISI 304L stainless steel tested in uniaxial tension-compression fatigue.

Fig. 5 shows, as an example, the distribution of the specific energy flux per cycle q measured along the boundary of V_c (R_c=0.52 mm) at different applied ΔK values; q is obtained by simply dividing h by f_L.

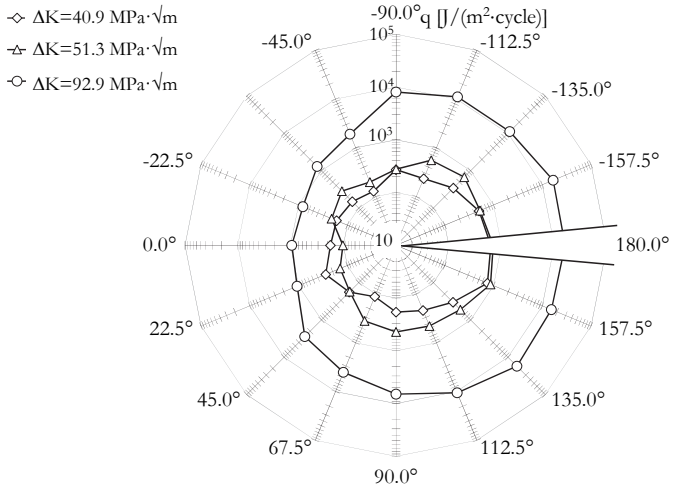

Figure 5: Distribution of the specific energy flux per cycle q along the boundary of structural volume V_c at different ΔK values (specimen V_45_R01_17).

CRACK GROWTH DATA

Fig. 6a shows a typical crack configuration captured by the digital microscope during a fatigue test. The raw crack propagation data are shown in Fig. 6b. Having the crack length vs the number of cycles, the crack growth rate da/dN was calculated. The Peak Stress Method [16] was adopted to evaluate the Mode I Stress Intensity Factor

(SIF) range, $\Delta K=K_{max}-K_{min}$, for different crack lengths. In view of this, linear elastic, two-dimensional, finite element analyses were performed by using the 4-node SOLID182 element of ANSYS® commercial code. To account for the machine grip effect, displacements were applied in the numerical model to the appropriate lines shown in Fig. 2a.

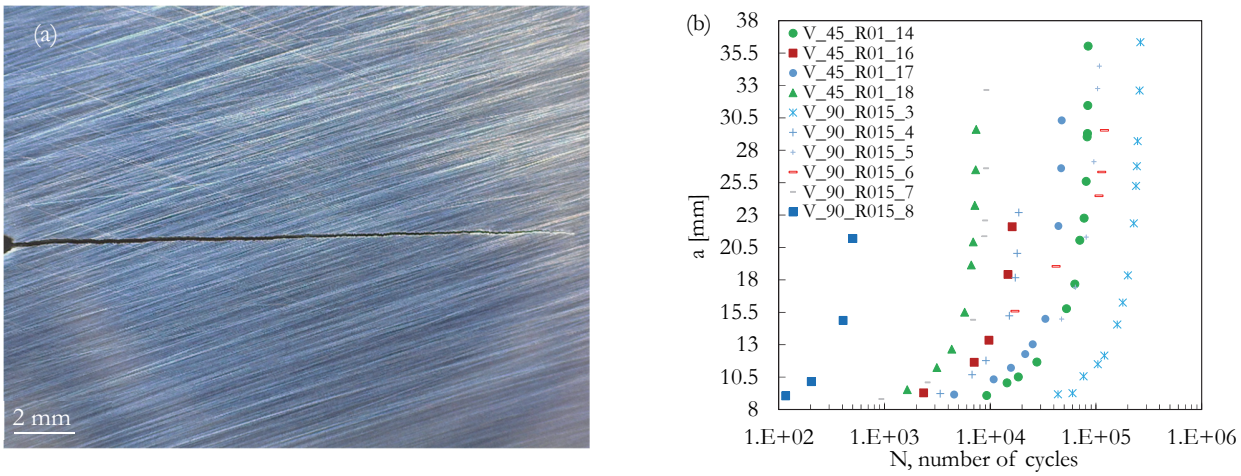

Figure 6: a fatigue crack observed during the tension-compression fatigue tests, (a=25.60 mm, $\Delta K=61.77$ MPa·m$^{0.5}$, $f_L=30$ Hz) (a) and crack propagation data (b).

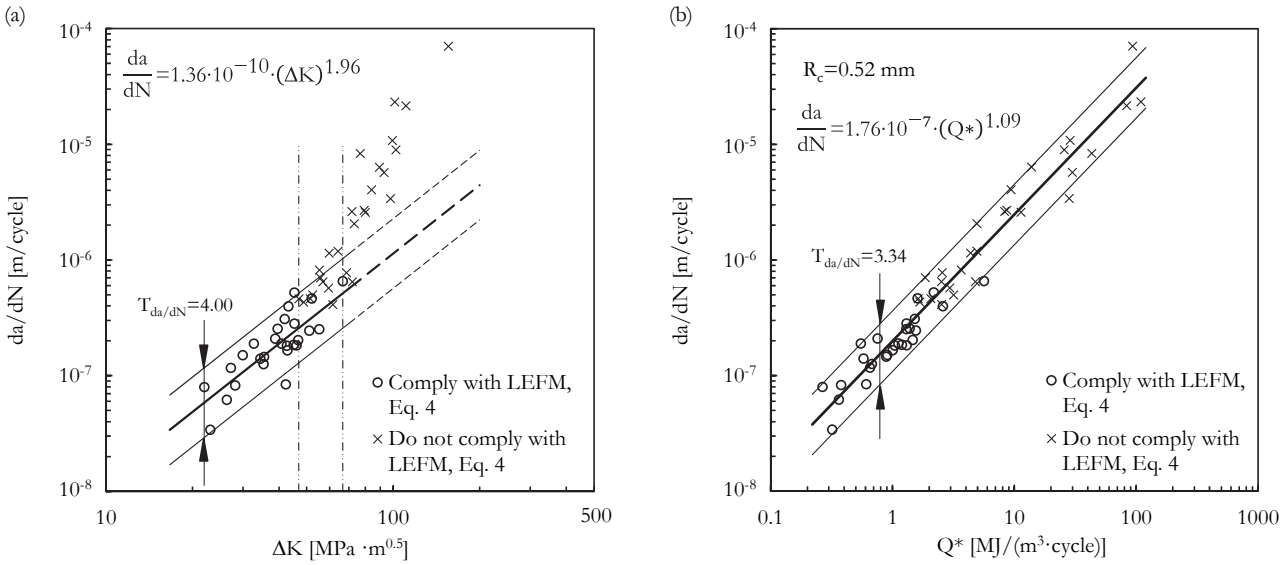

Figure 7: Crack growth rates vs ΔK (a) and Q* evaluated by using $R_c=0.52$ mm (b).

Fig. 7a shows the Paris curve of AISI 304L stainless steel, along with the 10%-90% scatter band and the crack growth rate scatter index $T_{da/dN}$ ($T_{da/dN}=4.00$), calculated under the hypothesis of log-normal distribution of da/dN.
In the same figure, a vertical band defined by two dashed vertical lines is reported, on the left hand side of which all data points satisfy the conditions of applicability of the LEFM according to Eq.4 [17], while on the right hand side of the band they do not:

$$a,(w-a),L \geq \frac{4}{\pi}\cdot\left(\frac{\Delta K}{2\cdot\sigma'_{p,02}}\right)^2 \tag{4}$$

where a is the crack length, w the specimen width (w=46 mm, see Fig. 2a), 2L the specimen length (2L=90 mm, see Fig. 2a) and $\sigma'_{p,02}$ the cyclic engineering proof stress equal to 265 MPa [9]. The data that did not satisfy the condition of applicability of the LEFM were not included in the statistical analysis reported in Fig. 7a. One can note that on the right

hand side of the band included by the vertical lines, crack acceleration occurs, which was interpreted as the effect of the excessive plasticity around the crack tip [18].

SYNTHESIS BASED ON THE AVERAGED DISSIPATED ENERGY Q*

The same crack growth data previously plotted in Fig. 7a are shown in Fig. 7b. In this case, Q*, calculated using R_c=0.52 mm combined with the spatial gradient technique Eq. (2), was assumed as driving force for crack propagation. Fig. 7b reports the mean curve, the 10%-90% survival probability scatter bands and the scatter index $T_{da/dN}$. The crack growth rates can be rationalized with a higher level of accuracy using the averaged heat energy Q*, rather than the range of the linear elastic mode I SIF ΔK.

CONCLUSIONS

In this paper, the specific heat energy per cycle averaged in a structural volume surrounding the crack tip, Q*, was used as a fatigue parameter to correlate the crack growth data generated from 4-mm-thick, hot rolled AISI 304L stainless steel specimens, tested in fully reversed tension-compression fatigue . The size of the structural volume was defined by equaling the averaged heat energy in cracked and smooth specimens for the same fatigue life and it was found equal to 0.52 mm. The crack growth data were plotted in terms of range of the linear-elastic Mode I stress intensity factor, ΔK, as well as Q*. When presented in terms of ΔK, a 10%-90% survival probability scatter band calibrated on crack growth data complying with the conditions of applicability of the LEFM was determined; however, as it is well known, crack acceleration is observed at progressively higher applied ΔK values. Conversely, by using the averaged heat energy Q*, all crack growth data (irrespective of the applied ΔK) fall within a single 10%-90% survival probability scatter band having the same scatter index of the ΔK-based one. This outcome is interpreted with the intrinsic nature of the energy Q*, which accounts for crack acceleration due to excessive plasticity occurring at increasingly higher applied ΔK values.

ACKNOWLEDGMENTS

This work was carried out as a part of the project CODE CPDA145872 of the University of Padova. The Authors would like to express their gratitude for financial support.

REFERENCES

[1] Meneghetti, G., Analysis of the fatigue strength of a stainless steel based on the energy dissipation, Int. J. Fatigue, 29 (2007) 81–94. DOI: 10.1016/j.ijfatigue.2006.02.043.

[2] Meneghetti, G., Ricotta, M., The use of the specific heat loss to analyse the low- and high-cycle fatigue behaviour of plain and notched specimens made of a stainless steel. Eng. Fract. Mech., 81 (2012) 2–17. DOI: 10.1016/j.engfracmech.2011.06.010.

[3] Meneghetti, G., Ricotta, M., Atzori, B., A synthesis of the push-pull fatigue behaviour of plain and notched stainless steel specimens by using the specific heat loss. Fatigue Fract. Eng. Mater. Struct., 36 (2013) 1306-1322. DOI: 10.1111/ffe.12071.

[4] Meneghetti, G., Ricotta, M., Atzori, B., Experimental evaluation of fatigue damage in two-stage loading tests based on the energy dissipation. Proc IMechE Part C: J Mechanical Engineering Science, 229 (2015) 1280-1291. DOI: 10.1177/0954406214559112.

[5] Meneghetti, G., Ricotta, M., Atzori, B., A two-parameter, heat energy-based approach to analyse the mean stress influence on axial fatigue behaviour of plain steel specimens. Int J Fatigue, 82 (2016) 60-70. DOI: 10.1016/j.ijfatigue.2015.07.028.

[6] Neuber, H., Über die Berücksichtigung der spannungskonzentration bei festigkeitsberechnungen. Konstruction 20 (1968) 245-251.

[7] Klingbeil, NW., A total dissipated energy theory of fatigue crack growth in ductile solids. Int J Fatigue, 25 (2003) 117–128.
[8] Meneghetti, G., Ricotta, M., Evaluating the heat energy dissipated in a small volume surrounding the tip of a fatigue crack. Int. J. Fatigue, 92 (2016) 605-615. DOI: 10.1016/j.ijfatigue.2016.04.001.
[9] Meneghetti, G., Ricotta, M., Rigon, D., The heat energy dissipated in a control volume to correlate the fatigue strength of severely notched and cracked stainless steel specimens. Proceedings of Fatigue 2017, 3-5 July 2017, Cambridge (UK).
[10] Peterson, RE., Notch sensitivity, in: G. Sines and J. L. Waisman (Eds.) Metal Fatigue, MacGraw-Hill, New York, (1959) 293-306.
[11] Tanaka, K., Engineering formulae for fatigue strength reduction due to crack like notches. Int J Fract, 22 (1983) R39–46.
[12] Sheppard, SD., Field effects in fatigue crack initiation: long life fatigue strength. Trans ASME, Journal of Mechanical Design, 113 (1991) 188-94.
[13] Taylor, D., Geometrical effects in fatigue: a unifying theoretical model. Int J Fatigue 21 (1999) 413–20.
[14] Lazzarin, P., Zambardi, R., A finite-volume-energy based approach to predict the static and fatigue behavior of components with sharp V-shaped notches, Int J Fract 112 (2001) 275–98.
[15] Meneghetti, G., Ricotta, M., Atzori, B., The heat energy dissipated in a control volume to correlate the fatigue strength of bluntly and severely notched stainless steel specimens, Structural Integrity Procedia, 2 (2016) 2076-2083.
[16] Meneghetti, G., Lazzarin, P., Significance of the Elastic Peak Stress evaluated by FE analyses at the point of singularity of sharp V-notched components, Fatigue Fract. Eng. Mater. Struct, 30 (2007) 95-106. DOI: 10.1111/j.1460-2695.2006.01084.x
[17] Dowling, N.E., Mechanical behavior of materials, Pearson Prentice Hall (2007).
[18] Tanaka, K., Takahash, H., Akiniwa, Y., Fatigue crack propagation from a hole in tubular specimens under axial and torsional loading, Int J Fatigue 28 (2006) 324-334. DOI: 10.1016/j.ijfatigue.2005.08.001

NOMENCLATURE

a: notch depth plus notch-emanated crack length [mm]
A%: percent deformation after fracture
f_{acq}: sample rate of the infrared camera [Hz]
f_L: load test frequency [Hz]
h: specific heat flux [W/m^2]
HB: Brinell hardness
K, ΔK: stress intensity factor, its range [MPa·√m]
q: specific energy flux per cycle [J/(m^2·cycle)]
Q, Q*: specific heat energy per cycle, its average value inside V_c [J/(m^3·cycle)]
r_n: notch radius [mm]
R: nominal stress ratio (ratio between the minimum and the maximum applied nominal stress)
R_c: radius of structural volume V_c [m]
$R_{p,02}$: engineering proof stress [MPa]
R_m: engineering tensile strength [MPa]
S_{cd}: external surface of control volume through which heat Q is transferred by conduction [m^2]
T_a: amplitude of temperature oscillations [K]
T_m: material temperature averaged over time [K]
V_c: structural volume [m^3]
z: specimen thickness [m]
2α: notch opening angle [rad]
λ: material thermal conductivity [W/(m·K)]
σ_{A-1}: plain material fatigue limit for R=-1 [MPa] (obtained from a stair-case sequence at 10^7 cycles)
$\sigma'_{p,02}$: cyclic engineering proof stress [MPa]